

Supporting Information

1. Experimental Section:

1.1 Materials:

Sodium hydroxide (NaOH) and hydrochloric acid (HCl) were obtained from Beijing Chemical Reagent Co. Potassium hydroxide (KOH) was obtained from Xilong Chemical Co., Ltd. Acetaldehyde (2 vol% in N₂) and CO₂ (2 vol% in N₂) were obtained from Beijing Chemical Co. All chemicals were analytical grade and used without further purification. Triply distilled water was used in all experiments.

1.2 Characterization

X-ray diffraction (XRD) characterization was carried out on a Rigaku D/max-2500 X-ray diffractometer. Morphology and composition analyses were carried out on a FEI quanta 250 field emission scanning electron microscopy (FESEM). High-resolution electronic micrographs were acquired using a JEOL JEM-2100 transmission electron microscope (TEM) operated at an acceleration voltage of 200 kV. UV-Vis diffusion reflectance (DR) spectra were recorded on a Lambda 900 UV-vis-NIR spectrophotometer, using BaSO₄ as reference. N₂ adsorption/desorption isotherms were measured at 77 K using a Micromeritics ASAP 2010N analyzer. Specific surface areas were calculated using the BET model. Photoluminescence (PL) spectra were recorded with a Jobin Yvon HR800 micro-Raman spectrometer using a 325 nm line from a He-Cd laser as excitation source. The binding energy level was determined by measuring X-ray photoelectron spectroscopy (XPS, an ESCA-LAB220i-XL electron spectrometer from VG Scientific using 300W Al K α radiation). Mott-Schottky analysis was performed in a conventional thermostatted (25 °C) three-

electrode cell in the dark, with a 1.44 cm² platinum flag as counter electrode and a saturated calomel electrode as reference. The working electrode was a TiO₂ thin film prepared as follows: the TiO₂ power was well supersonic dispersed with water and the suspension was applied on an indium-doped tin oxide conducting glass (ITO), 1.5*1.5 cm², by drop casting. The experiment was performed in aqueous 0.5 M Na₂SO₄ solution at pH≈7. The potential was systematically varied between 0.5 and -1.1V (vs NHE)with the frequency range being modulated between 500 to 3000 Hz by a PARSTAT 2273 advanced electrochemical system (Princeton Applied Research).

Measurement of transient photovoltage is as previously reported [Wei et al, J. Phys. Chem. C, 2011, 115, 8637]. The sample chamber consisted of a platinum wire gauze electrode (with the transparency of ca. 50%) as top electrode, a glass substrate covered with ITO as bottom electrode, and a 10 μm thick mica spacer as electron isolator. The samples were excited with a laser radiation pulse (wavelength of 355 nm and pulse width of 5 ns) from a third harmonic Nd:YAG laser (Polaris, New Wave Research, Inc.). Intensity of the pulse was regulated with a neutral gray filter and determined by an EM500 single-channel joulemeter (Molelectron, Inc.). The TPV signals were registered by a 500-MHz digital phosphor oscilloscope (TDS 5054, Tektronix) with a preamplifier. Electrical paramagnetic resonance (EPR) spectra were obtained using a CW-EPR Bruker EIEXSYS spectrometer in the X band (9.38 GHz) at 90 K equipped with a cylindrical cavity operating at a 100 kHz field modulation. The irradiation light source was a Xe lamp (Hayashi LA-410) and transmitted into the EPR cavity through an optical fiber.

1.3 Photocatalytic tests

Hydrogen production: The photocatalytic reactions of the photocatalysts were carried out in an outer irradiation-type photoreactor (Pyrex glass) connected to a closed gas-circulation system. 0.10 g of the photocatalysts were dispersed by a magnetic stirrer in 100 mL deionized water, where 10 mL methanol and 1 wt% Pt particles was contained. The suspension is thoroughly degassed to remove air and irradiated using a 300 W Xe-lamp (MICROSOLAR 300, Beijing Perfectlight Co., Ltd). The photocatalytic H₂ evolution rate was analyzed using an online SP-6890 gas chromatograph (GC, TCD detector, 5 A° molecular sieve columns and N₂ carrier).

Acetaldehyde degradation: Photocatalytic activity of samples was evaluated by the degradation of acetaldehyde in gas phase. 0.025 g powders were uniformly spread in a sample holder with a geometric area of 3.14 cm², which was placed on the bottom of a 500 mL cylinder-type Pyrex glass vessel. The glass vessel was flushed with O₂(20%)/N₂ gas to remove carbon dioxide from the system, and the relative humidity of atmosphere inside the vessel was controlled to 45% by passing the O₂/N₂ gas through chilled water. 5 mL acetaldehyde was introduced into the reaction vessel using a Pressure-Lock syringe to reach a concentration of 200 ppmv. After keeping in the dark for 10 min, the glass vessel was irradiated from top by a 200 W UV lamp (Hayashi UV410, wavelength range of 320–400 nm with a peak at 352 nm) which emitted UV light with an irradiance of 1.3 mW/cm² as measured with a power meter (Photoelectric instrument factory of Beijing normal university). The degradation of acetaldehyde and the generation of carbon dioxide were monitored using a gas

chromatograph (SP-2100A, BFRL Co.), equipped with a 2 m Porapak-Q column and a flame ionization detector.

2. Possible Mechanism of Maintenance of TiO₂ Nanotubes at High Temperature

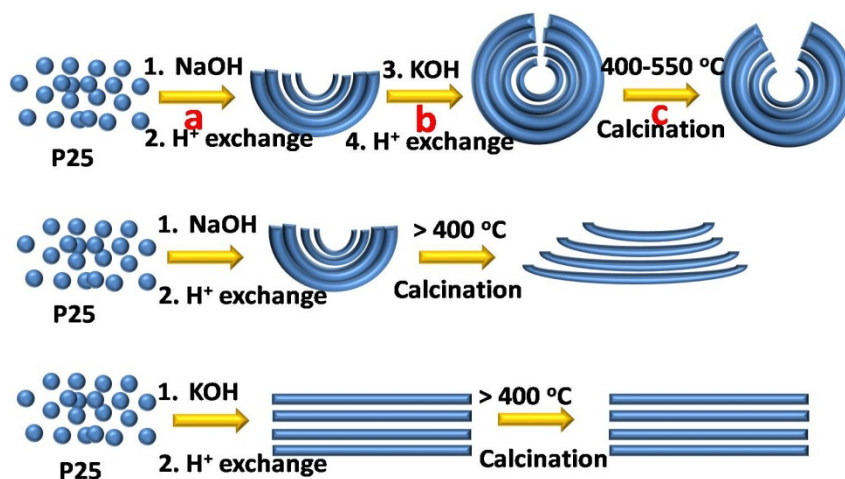
Up until now, it is agreed that the process of transformation of raw TiO₂ or titanium metal to nanotubular titanate occurs via the following stages^[12]: (i) partial dissolution of raw TiO₂ or titanium metal accompanied by epoxial growth of layered nanosheets of alkaline titanates; (ii) crystallization of dissolved titanates on nanosheets, which induces the curving and wrapping nanosheets to nanotubes because of the mechanical tensions; (iii) growth of nanotubes along the length, and (iv) exchange of alkaline metal ions by protons and transformation to TiO₂ nanotubes. To understand the formation mechanism of TiO₂ nanotubes in the as-employed two-step alkaline hydrothermal route in this work, we perform two comparative experiments. The first experiment is conducted in 10 M NaOH at 130 °C for 36 h, followed by proton exchange (the first step in the synthesis route). At this stage, the products displayed the nanotubular morphology. However, when subjected to calcination at 450 °C, the nanotubular morphology unfortunately disappeared. This is consistent with the previously reported results.^[13] We also only obtain TiO₂ nanosheets by alkaline hydrothermal reaction between Ti plate and NaOH solution, followed by proton exchange and calcinations,^[14] which further confirms that the common synthesis route in sole NaOH solution fails to produce TiO₂ nanotubes after high temperature treatment. The second experiment is conducted in 15 M KOH at 200 °C for 24 h and subsequently kept at 150°C for 12 h, followed by proton exchange (the second step in

the synthesis route). Differently, the products display nanofibrous morphology rather than nanotubes at the initial stage before calcination. In fact, because the solubility of TiO_2 in KOH solution is higher than in NaOH, it was usually to reduce the temperature during synthesis in order to keep the mechanical tension over titanate nanosheet and produce nanotubes. For example, Titanate nanotubes could be obtained at temperature as low as 56 °C in 10 M KOH solution for 12 days. However, only a yield of approximately 20–40% of nanotubes could be achieved, and the nanotubes were weakly crystallized.^[15] On the contrary, at higher temperature range (150-180 °C), the rate of crystallization of potassium titanate was large enough.^[16,17] As such, the thickness of nanosheet could exceed a critical value when they become too robust to bend before curving, leading to nanofibers instead of nanotubes. Accordingly, we tentatively conclude that the stability of TiO_2 nanotubes is synergistically induced by the concentrated NaOH and KOH solution, as illustrated in Scheme S1. The asymmetry environment around titanate nanosheet precursor may dominate the abnormal stability of TiO_2 nanotubes at high temperature. Specifically speaking, at the first stage, P25 TiO_2 reacts with concentrated NaOH to produce sodium titanate nanosheet segments. In the subsequent proton exchange process, due to the imbalance environment imposed by H^+ or Na^+ ion on two different side of a nanosheet, the nanosheets tends to bend and appear as multiwall nanotubes being not completely closed (step a). At the following stage, drastic reaction conditions of higher concentration of alkaline solution and higher temperature (15 M KOH, 200 °C) lead to dissolution of pre-formed titanic acid and further recrystallization in terms of epoxial

growth along the titanate acid nanotube. Owing to the imbalance environment imposed by K^+ or H^+ , both sides of nanosheets have different values of free surface energy. In order to compensate imbalance in surface tensions, the plane further to bend to produce multiwall nanotubes being almost closed (step b). Such hypothesis can be confirmed by the TEM image (Figure S3) of the potassium/hydrogen titanate precursor intermediates, which was collected from the products after 12 h reaction between KOH and titanate acid at 200 °C. Owing to the large surface tension imposed on the individual nanosheet in the nanotubes, the nanotubular morphology can be largely maintained despite of the decrease of the surface tension to some extent to reduce the surface energy upon last calcinations at higher temperature range from 450 to 550 °C (step c). Additionally, the high crystallization of titanates at high temperature (200 °C) is beneficial to topotactic transformation from titanates to TiO_2 (B) to anatase during thermal treatment and thereby anatase/ TiO_2 (B) heterojunction.^[18] Last, to help to understand the proposed mechanism illustrated in Scheme S1, comparative morphology evolution from titanate to TiO_2 nanostructure only via NaOH or KOH involved process are also given.

Table S1: Comparison of structural characteristics of as-synthesized samples in this work with that of others.

Reference	Calcination Temperature (°C)	As-calcined TiO ₂ products from titanate precursor	Surface area (m ² /g)	Phase composition	TiO ₂ (B) Content (%)
This Work	450	Nanotubes	277	Anatase+TiO ₂ (B)	48.11
	550	Nanotubes+Nanorods	168	Anatase+TiO ₂ (B)	7.44
Ref. 1	450	Nanofibers	55	Anatase+TiO ₂ (B)	17
Ref. 2	500	Nanowires	58.2	Anatase+TiO ₂ (B)	No data
Ref. 3	500	Nanofibers	39.0	Anatase+TiO ₂ (B)	No data
Ref. 4	550	Nanofibers	23.4	Anatase+TiO ₂ (B)	97.1
Ref. 5	600	Nanofibers	39	Anatase+TiO ₂ (B)	No data
Ref. 6	600	Nanobelts	20.78	Anatase+TiO ₂ (B)	40
Ref. 7	500	Nanotubes	106	Anatase	No data
	600	Nanobelts	15	Anatase+TiO ₂ (B)	No data
Ref. 8	500	Nanowires	19.4	Anatase+TiO ₂ (B)	No data
Ref. 9	600	Nanoribbons	31.6	Anatase+TiO ₂ (B)	ca. 80
Ref. 10	400	Nanotubes	132	TiO ₂ (B)	100
Ref. 11	400	Nanofibers	20	TiO ₂ (B)	100



Scheme S1: Scheme illustration for the formation mechanism of TiO₂ nanotubes with high thermal stability. The models are depicted from side view of the nanostructures.

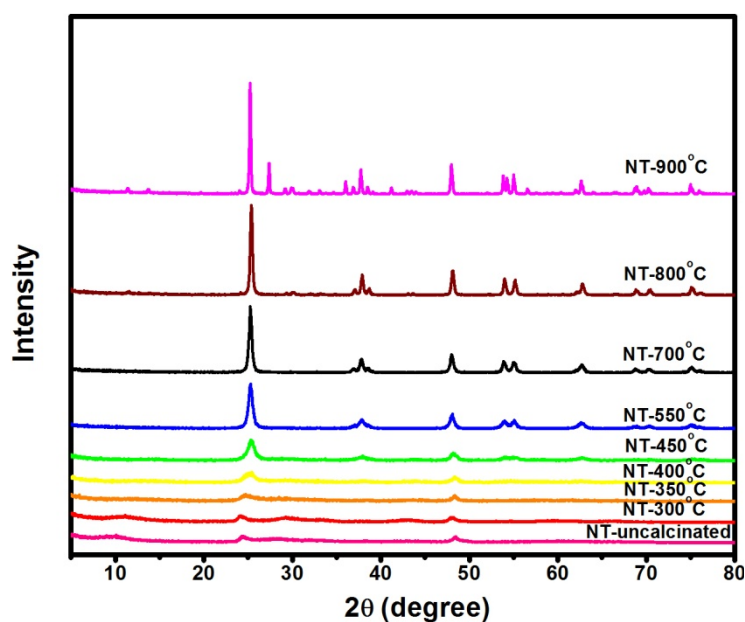


Figure S1: XRD patterns of nanotubes undergone no calcination and calcination from 300 to 900 °C for 2 hours.

Figure S1 displays the XRD patterns of nanotubes calcined from 300 to 900°C for 2 hours. Both the anatase and rutile phases were formed in NT-900°C, and no rutile phase was found in NT-700°C. So, NT-700°C can be chosen as pure anatase phase. Employing Scherer's equation, crystal sizes of 11.9, 17.6, 23.1 and 33.6 nm can be estimated for NT-450 °C, 550 °C , 700 °C and 800 °C samples, respectively,.

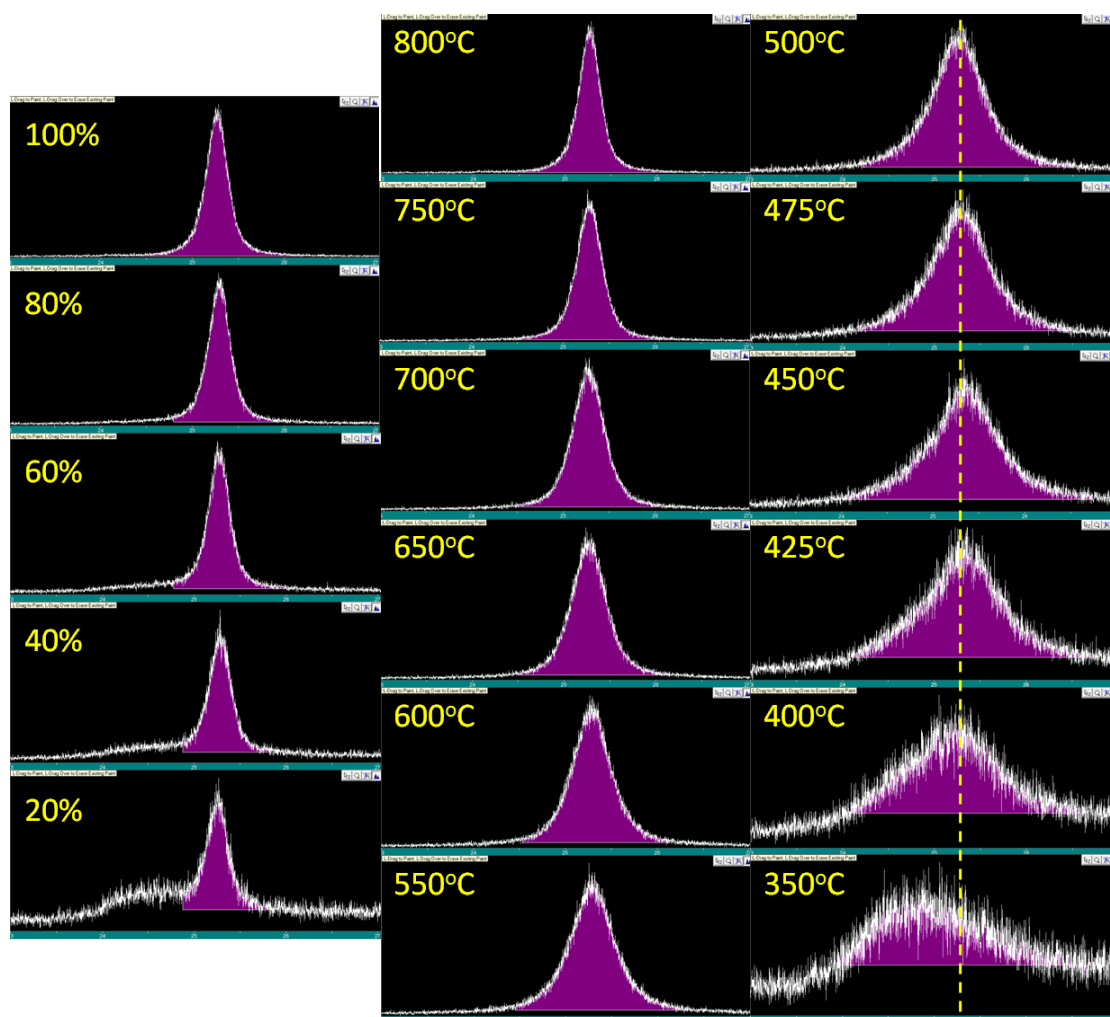


Figure S2: X-ray integrated intensities peak at 25.3° in the mixtures of known composition (as the standard) and heat-treated samples

Figure S2 shows the X-ray integrated intensities peak at 25.3° in the mixtures of known composition (as the standard) and heat-treated samples. The standard mixtures were prepared by pure anatase phase and pure $\text{TiO}_2(\text{B})$, mixed with 1:4, 2:3, 3:2, 4:1, 1:0 ratios and ground carefully to mix sufficiently. The corresponding integrated intensities are 93453, 76208, 55182, 35993, 17395, respectively. The heat-treated samples were prepared by calcining from 350 to 800 °C for 2 hours. We observed a shift to large angle of the diffraction peak for sample calcinated at 450 or 425 °C in

comparison with that calcined at 400 °C. In other words, for the samples calcined below 450 °C, the integral curve is asymmetric, which is due to the presence of TiO₂(B) phase. After removing the background of diffraction profile and dealing with the diffraction intensity of TiO₂(B) phase peak, the corresponding integrated intensities are 93453, 93832, 93755, 90314, 89886, 86956, 80897, 64373, 48500, 28052, 14444 for samples calcined at 800, 750, 700, 650, 600, 550, 500, 475, 450, 425, 400°C, respectively.

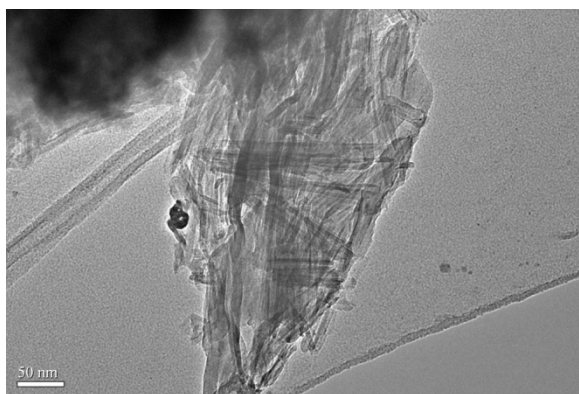


Figure S3: TEM image of intermediate product after KOH hydrothermal treatment for 12 h. Obviously, there is a black circle in the middle of the image. It implies that the multiple layered nanosheets in the nanotubes tend to curve to completely close, thereby leading to multiwall nanotubes.

References:

1. D. Yang, H. Liu, Z. Zheng, Y. Yuan, J. Zhao, E. R. Waclawik, X. Ke, and H. Y. Zhu, *J. Am. Chem. Soc.* 2009, 131, 17885-17893.
2. J. Jitputti, Y. Suzuki, S. Yoshikawa, *Catal. Commun.* 2008, 9, 1265-1271.

3. W. Li, Y. Bai, C. Liu, Z. Yang, X. Feng, X. Lu, N. K. Van Der Laak, K. Y. Chan, *Environ. Sci. Technol.*, 2009, 43, 5423-5428.
4. Z. Zheng, H. Liu, J. Ye, J. Zhao, E.R. Waclawik, H. Zhu, *J. Mol. Catal. A*, 2010, 316, 75-82.
5. W. Li, C. Liu, Y. Zhou, Y. Bai, X. Feng, Z. Yang, L. Lu, X. Lu, K. Chan, *J. Phys. Chem. C*, 2008, 112, 20539-20545.
6. W. Zhou, L. Gai, P. Hu, J. Cui, X. Liu, D. Wang, G. Li, H. Jiang, D. Liu, H. Liu, J. Wang, *CrystEngComm* 2011, 13, 6643-6649.
7. K. Kiatkittipong, J. Scott, R. Amal, *ACS Appl. Mater. Interfaces*, 2011, 3, 3988-3996.
8. B. Liu, A. Khare, E. S. Aydil, *ACS Appl. Mater. Interfaces* 2011, 3, 4444-4450.
9. N. Fu, Y. Wu, Z. Jin, G. Lu, *Langmuir*, 2010, 26, 447-455.
10. H. L. Kuo, C. Y. Kuo, C. H. Liu, J. H. Chao, C. H. Lin, *Catal. Lett.*, 2007, 113, 7-12.
11. S. Pavasupree, Y. Suzuki, S. Yoshikawa, R. Kawahata, *J. Solid State Chem.*, 2005, 178, 3110-3116.
12. D. V. Bavykin, J. M. Friedrich, F. C. Walsh, *Adv. Mater.* 2006, 18, 2807-2824.
13. Jr. E. Morgado, M. A. S. de Abreu, O. R. C. Pravia, B. A. Marinkovic, P. M. Jardim, F. C. Rizzo, A. S. Araujo, *Solid State Sci.* 2006, 8, 888-900.
14. C. H. Wang, X. T. Zhang, Y. L. Zhang, Y. Jia, J. K. Yang, P. P. Sun, Y. C. Liu, *J. Phys. Chem. C* 2011, 115, 22276-22285.
15. D. V. Bavykin, B. A. Cressey, F. C. Walsh, *Aust. J. Chem.* 2007, 60, 95-98.

16. G. H. Du, Q. Chen, P. D. Han, Y. Yu, L. M. Peng, *Phys. Rev. B* 2003, 67, 035323-1-035323-7.
17. X. Sun, X. Chen, Y. Li, *Inorg. Chem.* 2002, 41, 4996-4998.
18. W. Zhou, L. Gai, P. Hu, J. Cui, X. Liu, D. Wang, G. Li, H. Jiang, D. Liu, H. Liu, J. Wang, *CrystEngComm* 2011, 13, 6643-6649.